

Novel Radiomic Features based on Joint Intensity Matrices for Predicting Glioblastoma Patient Survival Time

Ahmad Chaddad, Paul Daniel, Christian Desrosiers, Matthew Toews, Bassam Abdulkarim

Abstract— This paper presents a novel set of image texture features, generalizing standard grey-level co-occurrence matrices (GLCM) to multi-modal image data through joint intensity matrices (JIMs). These are used to predict the survival of glioblastoma multiforme (GBM) patients from multi-modal MRI data. The scans of 73 GBM patients from the Cancer Imaging Archive are used in our study. Necrosis, active tumor and edema/invasion sub-regions of GBM phenotypes are segmented using the co-registration of contrast enhanced T1-weighted (CE-T1) images and its corresponding fluid-attenuated inversion recovery (FLAIR) images. Texture features are then computed from the JIM of these GBM sub-regions, and a random forest model employed to classify patients into short or long survival groups. Our survival analysis identified JIM features in necrotic (e.g., entropy and inverse-variance) and edema (e.g., entropy and contrast) sub-regions that are moderately correlated with survival time (i.e., Spearman rank correlation of 0.35). Moreover, 9 features were found to be associated with GBM survival, with a Hazard-ratio range of 0.38–2.1 and a significance level of $p < 0.05$ following Holm-Bonferroni correction. These features also led to the highest accuracy in a univariate analysis for predicting the survival group of patients, with AUC values in the range of 68–70%. Considering multiple features for this task, JIM features led to significantly higher AUC values than those based on standard GLCMs and gene expression. Furthermore, an AUC of 77.56% with $p=0.003$ was achieved when combining JIM, GLCM and gene expression features into a single radiogenomic signature. In summary, our study demonstrated the usefulness of modeling the joint intensity characteristics of CE-T1 and FLAIR images for predicting the prognosis of patients with GBM.

Index Terms— GBM, Joint histogram, radiomic, Survival analysis.

I. INTRODUCTION

Glioblastoma multiforme (GBM) is the most common and aggressive form of malignant primary brain tumor, occurring at a yearly rate of 2 to 3 cases per 100,000 adults in the USA and Europe [1]. The clinical outcome of GBM varies substantially, survival times following diagnosis ranging from weeks to decades, with a median of 15 months, and less than 5% of patients surviving more than 5 years [2]. Despite the increasing ability of genomics to describe patient-specific characteristics linked with genetics, only a few genomic

markers have been integrated into the clinic for predicting tumor response and/or patient survival. Methylation of MGMT promotor remains the most predictive factor in defining patient cohorts that will respond to Temozolomide [3]. The IDH1 R132H missense mutation can also be used to identify the cohort of patients with longer survival [4]. Whilst various markers have been proposed, their success as prognostic biomarkers is impeded by the need to physically sample the patients' tumor. Establishing prognosis using imaging features derived from the whole tumor is thus an attractive approach that could overcome the limitations of current genomic methods.

Multi-parametric MRI is a highly useful imaging technique for GBM diagnosis and treatment planning [5]. A significant body of research has investigated automatic approaches using this type of data for the classification and characterization of GBM tumors [6, 7]. Many of these approaches are based on shape or texture features. Shape or geometrical descriptors typically encode morphological characteristics such as volume, area and length of GBM sub-regions (e.g., necrosis, edema, active tumor) segmented from aligned multi-parametric data [8, 9]. On the other hand, texture features describe patterns of heterogeneity in these segmented sub-regions, which may be linked to cellular anomalies within corresponding tissues. Such features are often derived from image filters like wavelets or Laplacian-of-Gaussians [10]. They provide information that is complementary to shape, and are widely employed in so-called *radiomic analysis* approaches that adapt pattern recognition techniques to medical image analysis [11].

Co-occurrence statistics of neighboring image intensities represent the finest-grain texture measurements available. A widely used methodology is to compute texture descriptors from grey-level co-occurrence matrices (GLCM) [10,13], via quantifier functions like entropy or energy [13]. Covariance between color channels has been shown to improve texture classification in natural images [14]. This idea has been generalized to multi-parametric medical image data, by computing GLCM textures independently from individual modalities [10,12,15] or from linear image combinations [16]. However, these strategies do not make full use of the information available in the joint intensity statistics of multiple,

Manuscript submitted September 23, 2017.
A.C. P.D. and B.A. are with the McGill University, Montreal, Canada (e-mail: ahmad.chaddad@mail.mcgill.ca).

A.C. C.D. and M.T. are with the Ecole de Technologie Supérieure, Montreal, Canada.
This work was supported by grant from Varian Medical System.

complementary image modalities.

The primary contribution of this paper is a generalization of GLCM textures to multi-parametric image data. Our approach considers the joint co-occurrence statistics of intensities in all pairs of available image modalities and all GBM sub-regions (i.e., active tumor, edema, necrosis). These joint intensity matrices (JIM) are described within a principled Bayesian framework, accounting for prior assumptions on variables of intensity, geometry and segmented tissue labels. JIM textures are equivalent to GLCM textures in scalar image data, however, they define a novel set of complimentary texture features in the case of multi-parametric image data. Joint intensity statistics are commonly used in multimodal image registration approaches such as those based on mutual information [17]. To our knowledge this is the first work proposing their use for tumor analysis and survival prediction.

The proposed multimodal and region-dependent approach is motivated by the distinctiveness of intensity distributions in different GBM sub-regions, which also vary across image modalities. As suggested in various studies [18, 19], texture features capture characteristics of intra-tumoral heterogeneity that may be related to tumor progression and outcome. Encoding the relationship between textures in different GBM sub-regions and modalities could thus improve the prediction of survival for GBM patients.

The rest of this article is structured as follows. Section 2 describes the population, image data and the proposed technique based JIM in detail. Section 3 provides experimental setup and results. Section 4 discusses our finding. Finally, Section 5 concludes with a summary of our work’s main contributions and results.

II. MATERIALS AND METHODS

The processing pipeline of our proposed method for predicting GBM survival from JIM texture features is illustrated in **Figure 1**. This pipeline is composed of 4 steps: 1) data acquisition involving gadolinium contrast-enhanced T1-weighted (CE-T1) and fluid-attenuated inversion recovery (FLAIR) images, 2) affine co-registration of multi-parametric images and manual labelling of GBM sub-regions, 3) GLCM and JIM texture feature extraction from sub-regions, and 4) univariate and multivariate analysis of survival. The following sections describe the steps of our pipeline in detail.

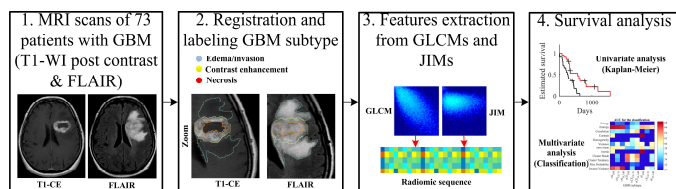


Fig.1. Proposed pipeline for predicting the survival of GBM patients, using GLCM and JIM texture features derived from multi-parametric MRI data (CE-T1 and FLAIR).

A. Population and Data Acquisition

The multi-parametric MRI data (CE-T1 and FLAIR) of 73 GBM patients were obtained from The Cancer Imaging Archive (TCIA) [20], a publicly available medical image repository.

The data used in our study are a subset of the TCGA-GBM database, corresponding to patients for which all three GBM sub-regions, i.e, necrosis (vN), contrast enhancement (vCE) and edema (vE), are present and clearly delineated. This requirement was necessary to ensure the proper segmentation of GBM sub-regions and to study the effect of textures in these sub-regions on prognosis. Many available patients in the database have no necrotic region, which is a key factor for the survival of GBM patients.

TABLE I
DEMOGRAPHIC INFORMATION OF STUDY POPULATION.

Gender	Male	43
	Female	30
Race	African American	4
	White	65
	Asian	2
	NA	2
Age	Min-max	18-84
	Median	61
	Mean	59.56
Karnofsky Performance Score	0-79	14
	80-100	46
	NA	13
Survival (censored)	< 358 days	36(3)
	> 358 days	37(7)
Radiation	Yes	61
	No	9
	NA	3

*NA is unknown

Since the TCGA-GBM database contains multisite data, the scanner model, pixel spacing, slice thickness and contrast varies within the selected cohort. To account for these differences, all volumes were resampled to a common voxel resolution of 1 mm³, for a total size of 512 × 512 × slices voxels (the slice number varying from one subject to another). Intensities within each volume were normalized to the [0,1] range. Finally, the survival in days, from time of scan to death (i.e., uncensored) or last visit (i.e., censored), was also provided for all 73 patients.

Patient demographic information is reported in Table I. The cohort of patients ranged in age from 18 to 84 years (median age of 61 years) with a median survival of 358 days and a median KPS of 90. A total of 61 patients received standard radiotherapy treatment (84%), 9 patients did not receive any radiotherapy, and the remaining 3 patients having no record of treatment. Forty-eight patients (66%) of patients received Temozolomide (TMZ) whilst 21 patients did not receive any chemotherapy (28%). No data was available for 4 patients regarding chemotherapy. There was considerable genetic diversity amongst samples (**Figure 1S** in **Appendix 1**), with the most prevalent genetic driver event being the mutation of CDKN2A (58%) followed by amplification of EGFR (47%). IDH1 R132H mutation was identified in only 2 patients, consistent with the low prevalence of this type of alteration in high grade glioma.

B. Labelling of GBM Sub-regions

To label GBM sub-regions, we co-registered the CE-T1 and

FLAIR images using a rigid transform model available in the 3D Slicer software² [21]. This step is required since images were generally acquired with different numbers of slices and at different angles. Following registration, GBM sub-regions were segmented (or labeled) manually in a slice-by-slice fashion by two experts (an oncologist and a research scientist) using 3D Slicer. An average Dice similarity coefficient over 87% was measured between the two sets of labels. A third expert (i.e., chief oncologist) reviewed these segmentations to produce the final labels. In this process, sub-regions were obtained by taking the overlap between corresponding contours in the two sets of labels and, when needed, correcting local inconsistencies (e.g., filling small holes).

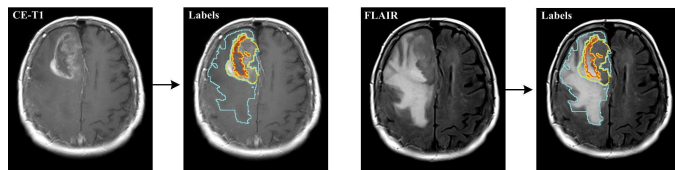


Fig. 2. Example of gadolinium CE-T1 and FLAIR images of a GBM patient. Original images and segmented tumor regions in CE-T1 and FLAIR. The region delineated by a yellow line corresponds to the active tumor or contrast enhancement (vCE) component, the inner region surrounded by the red line is necrosis (vN), and the outer region outlined in cyan is edema (vE). Note that the vCE and vN regions are more visible in the CE-T1 image, while the vE region is mostly visible in the FLAIR image.

As shown in **Figure 2**, necrosis and active tumor sub-regions can be determined from CE-T1 images, where the active tumor corresponds to contrast enhancing areas and necrosis to low intensity areas within (or near to) the active tumor. Edema/invasion sub-regions surround the active tumor and are generally identified more easily from FLAIR images.

C. Joint Intensity Matrix (JIM) Based Textures

Given a set of N multi-parametric images $\mathcal{M} = \{M_1, \dots, M_N\}$, we model the statistical relationship between voxel intensity I_a in image M_a and voxel intensity I_b in image M_b , occurring within GBM sub-region S , as a conditional joint density $p(I_a, I_b | S)$. Let $X \in \mathbb{R}^3$ be a 3D image location (i.e., voxel coordinate) and $T: \mathbb{R}^3 \rightarrow \mathbb{R}^3$ be a suitable invertible symmetric mapping between two coordinate systems (e.g. a diffeomorphism). This geometrical mapping is required in order to identify a set of joint intensity samples across image modalities, and may be obtained via image registration. This joint density can be expressed as

$$p(I_a, I_b | S) = \iint p(I_a, I_b | X, T, S) p(T | X, S) p(X | S) dT dX \quad (1)$$

where Equation (1) follows from Bayes' rule and the definition of marginalization. Factor $p(I_a, I_b | X, T, S)$ represents the conditional density of intensities (I_a, I_b) at locations $(X, T(X))$ within corresponding images, and for GBM sub-region S . Likewise, $p(T | X, S)$ models the range of variability in mapping T , conditioned on location X and GBM sub-region S , inside which texture-informative neighboring structure might be located. In the case of pre-aligned images,

$p(T | X, S)$ may be defined as a Gaussian density over the transformed coordinate $T(X)$ with zero mean and tissue-dependent covariance matrix Σ_S . Finally, $p(X | S)$ corresponds to a uniform density over voxel coordinates within sub-region S .

We define the joint intensity matrix $J_{a,b}^S$ as a discrete 2D representation of $p(I_a, I_b | S)$, where $J_{a,b}^S(i, j) \propto p(I_a = i, I_b = j | S)$ for discrete intensity levels i and j between 0 and 255. Computing $J_{a,b}^S$ from Equation (1) proceeds as follows. An outer summation is performed over the set $\Omega_S = \{X: p(X | S) > 0\}$ of locations X within sub-region S . An inner sum then integrates discrete co-occurrence information between intensity I_a at location X and intensity I_b at location $X + \delta$, where δ represents a neighborhood displacement. In this work, for every sub-region S , we considered a maximum displacement of one voxel for δ and a uniform probability for all voxels within this neighborhood. As mentioned above, JIMs could also be obtained using sub-region specific covariance matrices Σ_S . This refinement of the proposed approach is left for future work.

Several properties of JIMs are noteworthy. In the case of $a = b$, $J_{a,b}^S$ is equivalent to the standard GLCM representation computed in single-modality image data. Due to the symmetry of the image-to-image mapping T , $J_{a,b}^S = J_{b,a}^S$. Moreover, given N image modalities, there is a set of $N(N + 1)/2$ unique JIMs from which texture features are computed, N of those are standard GLCMs computed from individual modalities and $N(N - 1)/2$ represent additional joint intensity statistics across different modalities. **Figure 3** illustrates JIMs for a multi-parametric MRI dataset composed of CE-T1 and FLAIR images. It can be seen that each JIM reflects unique intensity co-occurrence information. The JIM approach generalizes the standard GLCM textures to multiple image modalities, generating texture features from joint intensity statistics between pairs of different image modalities.

D. Quantification of JIM Textures

The proposed JIMs are computed from intensities within the segmented GBM sub-regions of each image set. These intensities are quantized to 32 gray levels, resulting in 3 JIMs for each tissue sub-type S : two standard GLCMs from individual CE-T1 and FLAIR modalities and one representing the joint intensity statistics across these two modalities. For a single patient, there are thus 9 JIMs (i.e., 3 sub-regions \times 3 JIMs per sub-region). Each JIM is converted to a 11-element vector by applying the histogram quantifier functions proposed by Haralick [22]: Energy (f_1), Entropy (f_2), Correlation (f_3), Contrast (f_4), Homogeneity (f_5), Variance (f_6), Sum Mean (f_7), Cluster shade (f_8), Cluster tendency (f_9), Maximum Probability (f_{10}), and Inverse variance (f_{11}). Table II gives the formula for these quantifier functions. These features are now computed from JIMs, representing a novel class of texture features derived from joint intensity statistics.

E. Statistical Analysis, Classification and Prognosis

The usefulness of JIM features for GBM prognosis was

² <https://www.slicer.org/>

evaluated using the following univariate and multivariate analyses:

Feature correlation: We computed the Spearman’s rank correlation [23] between the 11 features extracted from each of GBM sub-regions and the survival time of the corresponding patient. The significance of these correlation values was measured as a p-values based on the null hypothesis that there is no correlation. An imputation strategy was used to account for censored patients (see below).

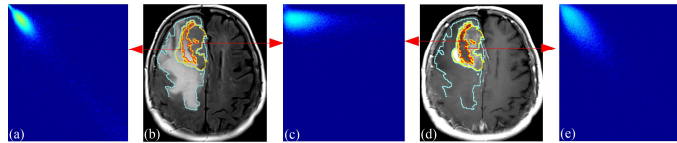


Fig. 3. The joint intensity matrices (JIMs) computed in multi-parametric MRI data consisting of FLAIR and CE-T1 modalities. (b) and (d) show segmentations of necrosis (red contour), contrast enhancement (yellow) and edema (cyan) GBM sub-regions. (a) and (e) give the JIMs corresponding to standard GLCMs of the necrotic sub-region in individual FLAIR and CE-T1 images. (c) shows the JIM of the same sub-region computed across FLAIR and CE-T1 images.

TABLE II
QUANTIFIER FUNCTIONS OF JIMS

Quantifier function	Formula
Energy	$f_1 = \sum_{i=1}^N \sum_{j=1}^N J_{a,b}(i, j)^2$
Entropy	$f_2 = -\sum_{i=1}^N \sum_{j=1}^N J_{a,b}(i, j) \log(J_{a,b}(i, j))$
Correlation	$f_3 = \frac{\sum_{i=1}^N \sum_{j=1}^N (i - \mu_i)(j - \mu_j) J_{a,b}(i, j)}{\sigma_x \sigma_y}$
Contrast	$f_4 = \sum_{i=1}^N \sum_{j=1}^N (i - j)^2 J_{a,b}(i, j)$
Homogeneity	$f_5 = \sum_{i=1}^N \sum_{j=1}^N J_{a,b}(i, j) / (1 + i - j)$
Variance	$f_6 = \sum_{i=1}^N \sum_{j=1}^N (i - \mu_i)^2 J_{a,b}(i, j) + (j - \mu_j)^2 J_{a,b}(i, j)$
Sum Mean	$f_7 = \frac{1}{2} \sum_{i=1}^N \sum_{j=1}^N (i J_{a,b}(i, j) + j J_{a,b}(i, j))$
Cluster Shade	$f_8 = \sum_{i=1}^N \sum_{j=1}^N (i + j - \mu_x - \mu_y)^3 J_{a,b}(i, j)$
Cluster Tendency	$f_9 = \sum_{i=1}^N \sum_{j=1}^N (i + j - \mu_x - \mu_y)^4 J_{a,b}(i, j)$
Max. Probability	$f_{10} = \max(J_{a,b})$
Inverse variance	$f_{11} = \sum_{i=1}^N \sum_{j=1}^N J_{a,b}(i, j) / (i - j)^2$
μ_x, μ_y, σ_x and σ_y are the means and standard deviation of partial probability density functions P_x and P_y ;	
$\mu_x = \sum_{i=1}^N \sum_{j=1}^N i \cdot J_{a,b}(i, j)$; $\mu_y = \sum_{i=1}^N \sum_{j=1}^N j \cdot J_{a,b}(i, j)$;	
$\sigma_x = \sqrt{\sum_{i=1}^N \sum_{j=1}^N (1 - \mu_x)^2 \cdot J_{a,b}(i, j)}$ $\sigma_y = \sqrt{\sum_{i=1}^N \sum_{j=1}^N (1 - \mu_y)^2 \cdot J_{a,b}(i, j)}$	

Kaplan-Meier feature analysis: We considered each feature (i.e., 11 JIM, 11 GLCM-CE-T1, and 11 GLCM-FLAIR) in turn and used the median value of this feature to separate patients in two groups: those with feature value less than the median, and those with feature value above or equal to the median. As in [24], we then computed the time-to-event (i.e., number of days from scan until death or last visit) distributions of the two groups using the Kaplan-Meier estimator, and compared them using the log-rank significance test.

Survival group feature differences: We grouped the patients into two groups, short survival time and long survival time, using the median patient survival time (i.e., 358 days) as the cut-off threshold. While other thresholding strategies may be used for defining these groups, the median has the important

advantage of giving even-sized groups, thus avoiding group size as potential bias in the analysis. A Wilcoxon rank sum test was then employed to assess the difference between the median value of each feature across these groups.

Survival group prediction: We considered GBM prognosis as a binary classification task between long and short survival time groups, defined by the median patient survival time (i.e., 358 days). Although various classifiers could be used for this task, we chose the random forest (RF) as it generally performs well when training data is limited [25]. By combining decision tree bagging with random feature subspace selection, it can thus reduce errors caused by training data variance and offers a good generalization to new data. Moreover, RF models can be used to inspect the features that are most dominant in classification.

We computed the area under the curve (AUC) obtained by the RF classifier for individual features and various feature combinations. A 5-fold cross-validation strategy was applied to obtain unbiased estimates of performance. In this strategy, training images are divided into 5 equal-sized subsets and, in each fold, one subset is put aside for testing and the remaining 4 subsets are used to train the RF classifier. Performance is reported as the mean AUC obtained across the 5 folds. We also measured the significance the predicted survival groups by applying the Kaplan-Meier estimator and log-rank test on these groups.

We compared the accuracy and significance obtained using the proposed JIM features with the one resulting from standard GLCM-CE-T1 and GLCM-FLAIR features. We also considered as features the alteration status of 11 genes that were shown to be associated with GBM survival [26]–[30]: IDH1, EGFR, PTEN, PDGFRA, MDM2, TP53, CDKN2A, NF1, CDK4, ATRX and PIK3CA. Prediction performance is reported for these features used as only input to the RF classifier, or in combination with GLCM/JIM features.

Except for the analysis based on the Kaplan-Meier estimator, other analyses cannot be used directly on censored data. To alleviate this problem, we considered a simple imputation strategy in which censored patients are assigned the mean survival time of uncensored subjects with a time-to-death greater or equal to their own time of last visit. We also repeated these analyses using only uncensored patients, to measure the effect of this strategy. The results obtained for censored data are provided in **Appendix 1**.

Furthermore, for the analysis of feature significance using Spearman correlation, the log rank test and the Wilcoxon rank sum test, the problem of multiple comparisons (11 quantifiers functions \times 3 GBM sub-regions \times 3 types of JIM features = 99 p-values) is dealt with using the Holm-Bonferroni method [31]. All the features were corrected using the Holm-Bonferroni correction. This correction technique is known to be uniformly more powerful than the standard Bonferroni method. For all experiments, statistical significance of features was assessed at $p < 0.05$ following Holm-Bonferroni correction.

III. EXPERIMENTAL RESULTS

A. Univariate Analysis of Radiomic Features

Figure 4 summarizes the univariate analysis of feature significance. **Figure 4 (top left)** shows the Spearman correlation values between features and the survival time of GBM patients (n=73). Mild correlation values in the range of 0.30-0.35 were found in necrotic (i.e. entropy and inverse-variance) and edema (i.e. entropy and contrast) sub-regions, while active tumor sub-regions showed low correlation values. Only JIM features showed significant correlation with survival time in edema sub-regions, with $p < 0.05$ following correction.

The heatmap of p-values (in $-\log_{10}$ scale) obtained from the log rank test is illustrated in **Figure 4 (top right)**. The values in this figure measure the difference in the survival profile of patients divided using the median value of each feature (patients below versus above the median value). We find a total of 9 features leading to statistically significant differences, which are derived from necrosis (i.e., entropy feature derived from JIM and FLAIR, and inverse variance features derived from JIM, CE-T1 and FLAIR) and edema sub-regions (i.e., entropy, contrast, and homogeneity features derived from JIM and inverse variance feature derived from CE-T1). Features derived from active-tumor/contrast-enhancement sub-regions were statistically non-significant.

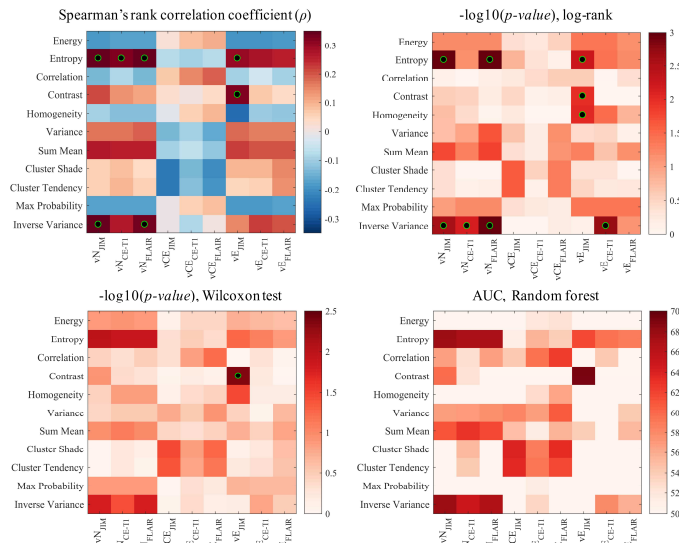


Fig.4. Analysis of texture features derived from GBM (i.e., 73 patients) regions (i.e. necrosis (vN), active tumor/contrast enhancement (vCE), and edema (vE)) using JIM, and GLCM (i.e. CE-T1 and FLAIR). **(Top left)** Heatmap of Spearman correlation values, color-coded from negative (dark blue) to positive (dark red). Green-black circles represent significant features with corrected $p < 0.05$. **(Top right)** Heatmap of p-values for the log-rank test comparing patients with feature values below or above the median. **(Bottom left)** Heatmap of Wilcoxon test p-values (in $-\log_{10}$ scale) comparing the distribution of features in short or long survival patient groups. Reported p-values are color-coded from non-significant (light blue) to highest significant (dark blue). Green-black circles identify significance features with corrected $p < 0.05$ **(Bottom right)** Heatmap of mean AUC obtained with individual features to predict the survival group of patients. Values are color-coded from lowest accuracy (dark blue) to highest accuracy (dark red).

Figure 4 (bottom left) gives the p-values (in $-\log_{10}$ scale) of the Wilcoxon rank sum test, comparing the distribution of each

feature short and long patient survival time groups. We observe a single significant feature with corrected $p < 0.05$: the JIM contrast feature derived from edema sub-regions. Moreover, the univariate analysis of survival prediction is summarized in **Figure 4 (bottom right)**, which gives the AUC values obtained by the RF classifier using individual features as input. It can be seen that the entropy feature derived from necrosis sub-regions (both JIM and CE-T1/FLAIR GLCM) and the JIM contrast feature from edema sub-regions are the most dominant features to discriminate

Table III

SUMMARY OF KAPLAN-MEIER ANALYSIS FOR SIGNIFICANT FEATURES (I.E., CORRECTED $P < 0.05$) DERIVED FROM NECROSIS AND EDEMA REGIONS

GBM region	Features / JIMs	Cut-off	Median Survival: (days)	
			Feature > Cut-off	Feature < Cut-off
Necrosis	Entropy/JIM	0.293	451.5	268
	Inverse-variance/JIM	0.050	483.5	285
	Inverse-variance/CE-T1	0.038	451.5	322
	Entropy/FLAIR	0.324	451.5	268
	Inverse-variance/FLAIR	0.030	451.5	279
Edema	Entropy/JIM	0.276	502.5	291
	Contrast/JIM	0.444	481	285
	Homogeneity/JIM	0.934	288	486
	Inverse-variance/CE-T1	0.024	502.5	291

between short and long survival patients, with AUC values between 68% and 70%.

Figure 5 provides the Kaplan-Meier curves of features that were shown to be significant using the log rank test. We observe that GBM patients with above-median values of entropy (JIM and FLAIR) and inverse-variance (JIM, CE-T1 and FLAIR) in necrosis sub-regions have higher survival rates than those with below-median values for these features, with hazard ratios of 0.36-0.41. Correspondingly, these patients have a median survival time of 451.5-483.5 days, compared to 268-322 days for other patients (**Table III**). In edema sub-regions, JIM features of homogeneity, contrast and entropy, as well as CE-T1 features of inverse-variance, also lead to marked differences in survival rates, with hazard ratio values in the range of 0.41-0.47.

B. Multivariate Analysis of Survival Prediction

Results of our multivariate survival prediction analysis can be found in **Figure 6a**, which gives the mean ROC curves and AUC values obtained by the RF classifier for various combinations of features. It can be seen that considering only genomic features yields a low accuracy, with a mean AUC of 60.20%. Adding the proposed JIMs to these features increases the mean AUC by over 15% to a value of 75.95%. Considering only radiomic features, JIMs provide a mean AUC improvement of 6.33% and 8.02% over GLCM-CE-T1 and GLCM-FLAIR features, respectively. Finally, the highest mean AUC of 77.56% is achieved when considering all features together (i.e., genes, GLCM-CE-T1, GLCM-FLAIR and JIM).

Table IV compares the prediction accuracy of different feature combinations using a one-side paired t-test. It can be seen that Genes+JIM significantly outperforms both the

Genes+GLCM-CE-T1 and Genes+GLCM-FLAIR combinations with $p < 0.05$, demonstrating the advantage of the proposed multi-modal features compared to the ones based on a single modality. Although combining gene features with JIM improves accuracy slightly compare to JIM alone, this difference is not statistically significant. Likewise, adding GLCM features to the combination of genes and JIM features does not yield any statistically significant improvement. In summary, results indicate that gene and GLCM features provide limited benefits over the proposed JIMs.

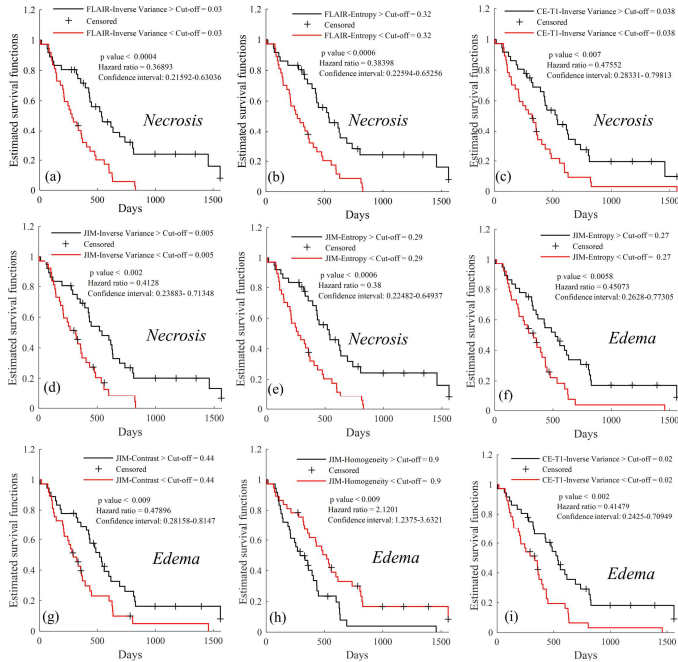


Fig. 5. Kaplan-Meier curves comparing the survival rate of GBM patients, partitioned into two groups using cut-off (median) of the significant features. Features derived from necrosis (a, b, c, d and e) and edema (f, g, h and i) regions as depicted in Figure 4b.

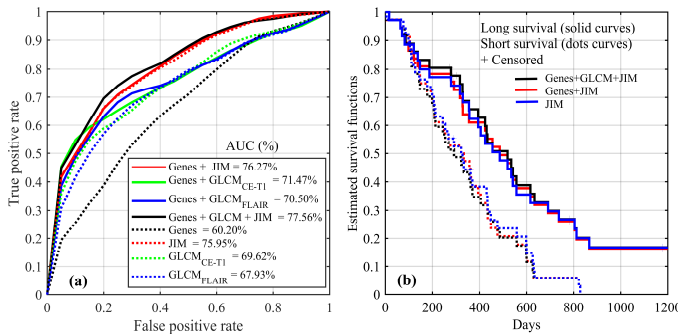


Fig. 6. (a) Mean ROC curves obtained by the RF model for discriminating between short and long survival time patients (using the median survival time as threshold). Results are reported for various imaging features and combinations of genomic, JIM and GLCM features. (b) Kaplan-Meier curves comparing the survival rate of patient groups predicted by the random forest classifier using different feature combinations as input.

In **Table V**, we report the results of the log-rank test using the binary prediction of the RF classifier to define patient groups. We see that all combinations involving JIM features (i.e., JIM, Genes+JIM or Genes+GLCM+JIM) lead to patient groups having significantly different survival profiles, with $p < 0.05$. On the other hand, no significant difference is observed for

groups obtained using combinations of gene and GLCM features alone. **Figure 6b** shows the Kaplan-Meier curves for patient groups obtained with JIM, Genes+JIM and Genes+GLCM+JIM feature combinations. We observe important differences in the survival functions of short survival patients compared to long survival patients. For instance, using only JIMs gives groups with a difference of 148 days in their median survival time and a hazard ratio of 2.01 (**Table V**). Moreover, we considered leave-one out cross validation (LOOCV) to fully examine the advantage of the JIM model. As shown in the previous validation (10-fold CV), LOOCV showed important differences in the survival functions of short survival patients compared to long survival patients. For example, using only JIMs, genes+JIM and genes+GLCM+JIM lead to groups with median survival time differences of 107, 176.5 and 197.5 days and hazard ratios of 1.88, 1.93 and 2.86, respectively (i.e., **Table V.S2 of Appendix 1**).

C. Analysis of Patients with Uncensored Survival Time or Radiation Therapy

In order to fully exploit available data ($n=73$ patients), the previous analyses applied an imputation strategy to include patients whose survival time is censored. To measure the impact of this factor, we repeated these analyses using only uncensored patients ($n=63$). Results can be found in **Figure 4.S1 of Appendix 1**, which shows the heatmaps of Spearman correlation values, log-rank test p-values, Wilcoxon test p-values and AUC obtained for individual features.

In general, results observed for uncensored patients are similar to those obtained using all patients with the imputation strategy. In most cases, the same features (quantifier function, GBM sub-region and modality) lead to the highest correlation, significance or accuracy in both cases. For instance, we also find mildly correlated features (0.26-0.27 correlation) in the necrotic (i.e., entropy and inverse-variance) and edema (i.e., entropy and contrast) sub-regions. As in the analysis on all patients, active tumor sub-regions showed low correlation values. Moreover, we observe higher accuracy (mean AUC) values for several features (e.g., energy in necrotic sub-regions) when limiting the analysis to uncensored patients. Conversely, significance decreases uniformly in the p-values of the correlation, log-rank and Wilcoxon analyses on uncensored patients. In both cases, these observations are most likely due to the lower number of patients ($n=63$ compared to $n=73$).

Another possible confound in our study is the type of treatment received by GBM patients. To account for this factor, we performed the proposed analyses considering only patients that received radiation therapy ($n=61$). Results are shown in **Figure 4.S2, Figure 5.S1, Figure 5.S2, Table III.S and Table V.S of Appendix 1**. Once more, we observe a pattern of features with highest correlation, significance and accuracy that is similar to the one obtained with all patients ($n=73$). Specifically, **Figure 5S1** provides the Kaplan-Meier curves of features that were shown to be significant using the log rank test. We observe that GBM patients with above-median values of entropy (FLAIR) and inverse-variance (FLAIR) in necrosis sub-regions have higher survival rates than those with below-median values for these features, with hazard ratios of 0.4-0.41. Similarly, these patients have a median survival time of 451.5

days, compared to 333 days for other patients (**Table III.S**). In edema sub-regions, JIM of entropy and homogeneity features lead to marked differences in survival rates, with hazard ratio value of 0.42 and 2.39, respectively.

As in the previous analysis of all the patients we considered ($n=73$), we see significant differences between short and long survival group of GBM patients that received treatment radiation (**Figure 5S2**). We found again that only the JIM, combined Genes+JIM and Genes+GLCM+JIM features are statistically significant with AUC (p-value) of 70.35 (0.01), 70.83 (0.003) and 71.25 (0.02), respectively. Comparing the previous findings in **Table V**, features derived from Genes+JIM and Genes+GLCM+JIM of GBM patients that received treatment radiation are more significant with p of 0.003 and 0.002, respectively (**Table V.S1**).

IV. DISCUSSION

While next-generation sequencing has been shown useful in predicting survival and tumor response to therapies in select cases, the inability to account for regional (intra-tumoral) heterogeneity has hindered advancement in identifying prognostic factors for GBM. For instance, despite the wealth of knowledge describing the role of EGFRvIII in driving an aggressive phenotype in pre-clinical models, translation of this marker to the clinic has been unsuccessful, with conflicting reports regarding its real prognostic value [32, 33]. Intra-tumoral heterogeneity of GBM may account for different subpopulations, which can limit the utility of even the best-validated driver events for prognostic usage [34]. Radiomic analysis offers the possibility of assessing abnormal heterogeneity throughout the whole tumor. Approaches based on this principle use quantitative imaging features to describe characteristics of underlying tissues that may be invisible to the human visual system [35–40].

Several studies have considered radiomic features for predicting the survival of GBM patients [15, 41–43]. In [42], 402 features (i.e., co-occurrence, grey-level dependence and directional gradients) derived from peritumoral brain zones were used to distinguish long versus short survival time in GBM patients. Likewise, such features (i.e., tumor shape, signal intensity, and texture) derived from the MRI data of 66 patients with GBM were shown to provide prognostic survival value [44]. Recently, studies have focused on combining imaging features with gene expression data, the resulting combination referred to as radiogenomic [45]. In [46], the volume of intra-tumoral GBM sub-regions has been shown to have a value to complementary genomics for predicting GBM survival. Tumor heterogeneity has also been assessed in various radiomic techniques in parallel with gene expression [47–52].

So far, the investigation of radiomic features extracted from multi-parametric data remains limited. We proposed novel features that capture the joint co-occurrence statistics of intensities in pairs of image modalities, and used these features to predict the survival of GBM patients. Our approach is motivated by the fact that GBM sub-regions (i.e., active tumor, edema, necrosis) are characterized by distinct intensity distribution, or textures, which vary across image modalities.

The significance of JIM features for GBM prognosis was measured using various analyses. Our analysis of correlation showed 5 features derived from of necrosis sub-regions and 2 features derived from edema sub-regions that were mildly correlated with survival outcome of GBM patients, all statistically significant with corrected $p < 0.05$ (**Figure 4 top left**). Likewise, our Kaplan-Meier analysis identified 9 features derived from necrosis and edema sub-regions exhibiting statistically significant associations with survival (**Figure 4 top right** and **Figure 5**). Finally, the analysis of group differences using the Wilcoxon sum rank test identified a single significant feature, derived from edema sub-regions (**Figure 4 bottom left**).

TABLE IV

P-VALUES OF ONE-SIDED PAIRED T-TEST COMPARING THE MEAN AUC OBTAINED FOR DIFFERENT FEATURE COMBINATIONS. THE ALTERNATIVE HYPOTHESIS IS THAT THE FEATURE COMBINATIONS IN COLUMNS GIVE A HIGHER MEAN AUC THAN THE ONES IN ROWS.

Features	Genes + JIM	Genes + GLCM + JIM
Genes + JIM	–	0.5
Genes + GLCM-CE-T1	0.02	0.0039
Genes + GLCM-FLAIR	0.01	0.0031
Genes	2.6×10^{-5}	7.6×10^{-6}
JIM	0.8	0.3
GLCM-CE-T1	0.006	0.0012
GLCM-FLAIR	0.005	0.0015

TABLE V

SUMMARY OF KAPLAN-MEIER ANALYSIS FOR PREDICTED PATIENTS GROUPS (I.E., SHORT VS. LONG SURVIVAL OUTCOME). THE MEDIAN SURVIVAL (MS) TIME, HAZARD RATIO (HR), 95% CONFIDENCE INTERVAL (CI) AND LOG-RANK P-VALUE ARE REPORTED.

Features	MS (days)		HR	CI	p
	short	long			
Genes + JIM	327.5	455	2.14	1.2-3.6	0.006
Genes + GLCM-CE-T1	344	434	1.69	1.02-2.7	0.053
Genes + GLCM-FLAIR	322	432	1.55	0.9-2.5	0.104
Genes + GLCM + JIM	291	444.5	2.29	1.3-3.8	0.003
Genes	366	333	1.09	0.6-1.7	0.820
JIM	306.5	455	2.01	1.2-3.3	0.011
GLCM-CE-T1	327.5	430	1.63	0.9-2.68	0.074
GLCM-FLAIR	327.5	424	1.42	0.87-2.3	0.192

The ultimate goal of this study is to define image biomarkers that are capable of predicting the survival of GBM patients. Toward this goal, we trained random forest classifiers using the proposed features to predict the survival time group (i.e., below or above the median survival time) of patients. The importance of individual features was first evaluated by using each of them as single input to the classifier. Dominant features, which are derived the JIMs of necrotic and edema sub-regions, were consistent with results from the Spearman correlation analysis, log-rank test and Wilcoxon significance test (**Figure 4 bottom right**). We then measured the prediction accuracy of various features combinations in a multivariate analysis. Our results showed that combining texture features and gene alteration status improved survival prediction accuracy. Likewise, our proposed JIM features led to improved predictions compared to classical GLCM features (**Figure 6a**). Overall, these findings suggest that JIM features, in particular those derived from necrosis and edema sub-regions, can help predict the survival

of GBM patients with higher accuracy than standard GLCM features (**Figure 6b** and **Table V**).

The results of our experiments are consistent with previous studies indicating the importance of texture features in edema sub-regions [53–55] and shape features in necrotic regions [55–58] for GBM prognosis. The low predictive power of gene alteration status, suggested by our results, has also been shown in the work of Jain et al. [59]. In this particular study, it was found that patients with relative cerebral blood volume of non-enhancing regions (i.e., edema regions) and EGFR mutation had significantly poor survival (log-rank test $p = 0.03$; random forest prediction $AUC=62\%$).

In terms of survival prediction accuracy, the proposed approach compares favorably with recent works. In [18], Liu et al. report an AUC of 81% for the classification of 133 GBM patients of the TCGA database into two survival groups (i.e., less or more than 1 year), using feature selection and SVMs. However, employing a fixed 1-year cut-off instead of the population median survival time leads to unbalanced classes which can bias the results. In a study by Park et al. [60] using a private dataset of 108 GBM patients, an integrated time-dependent AUC (iAUC) of 67% was obtained by considering both preoperative clinical and imaging features with the multivariate Cox proportional hazards model.

This study has several limitations which are worth mentioning. The number of subjects ($n=73$) is relatively low. While the primary goal of the study was to evaluate the usefulness of JIM features for GBM survival prediction, evaluating these features on a larger cohort would provide a more reliable assessment. Moreover, this study was limited to CE-T1 and FLAIR MRI data only. Additional MRI sequences, such as diffusion-weighted and susceptibility-weighted MR imaging could potentially improve the performance of the proposed method. Finally, as described in Section II.C, the proposed model could be extended to consider joint intensity distributions specific to each GBM sub-region and have longer-range interactions within larger voxel neighborhoods.

V. CONCLUSIONS

We presented a novel method for analyzing multi-parametric image data using joint intensity matrices (JIMs). These JIM features were evaluated in terms of their ability to predict GBM patient survival, using contrast enhancement, necrosis and edema tumor sub-regions extracted from CE-T1 and FLAIR MRI data. Our results demonstrate the usefulness of JIM features in discriminating between short and long survivors from a cohort of GBM patients, in particular features extracted from necrotic and edema sub-regions. The proposed technique could help clinicians determine prognosis and design optimal treatment plans for patients with GBM.

REFERENCES

[1] T. Koca et al., "Comparison of linear accelerator and helical tomotherapy plans for glioblastoma multiforme patients," *Asian Pac. J. Cancer Prev.*, vol. 15, no. 18, pp. 7811–7816, 2014.

[2] Q. T. Ostrom et al., "CBTRUS Statistical Report: Primary Brain and Central Nervous System Tumors Diagnosed in the United States in 2006–2010," *Neuro Oncol*, vol. 15, no. suppl 2, pp. ii1–ii56, Jan. 2013.

[3] K. Zhang, X. Wang, B. Zhou, and L. Zhang, "The prognostic value of MGMT promoter methylation in Glioblastoma multiforme: a meta-analysis," *Fam. Cancer*, vol. 12, no. 3, pp. 449–458, Sep. 2013.

[4] J. Cai et al., "Detection of ATRX and IDH1-R132H immunohistochemistry in the progression of 211 paired gliomas," *Oncotarget*, vol. 7, no. 13, pp. 16384–16395, Feb. 2016.

[5] L. S. Hu et al., "Multi-Parametric MRI and Texture Analysis to Visualize Spatial Histologic Heterogeneity and Tumor Extent in Glioblastoma," *PLOS ONE*, vol. 10, no. 11, p. e0141506, Nov. 2015.

[6] A. Chaddad, "Automated Feature Extraction in Brain Tumor by Magnetic Resonance Imaging Using Gaussian Mixture Models," *International Journal of Biomedical Imaging*, vol. 2015, pp. 1–11, 2015.

[7] B. H. Menze et al., "The Multimodal Brain Tumor Image Segmentation Benchmark (BRATS)," *IEEE Trans Med Imaging*, vol. 34, no. 10, pp. 1993–2024, Oct. 2015.

[8] Z. Zhang et al., "Identifying the survival subtypes of glioblastoma by quantitative volumetric analysis of MRI," *J Neurooncol*, vol. 119, no. 1, pp. 207–214, May 2014.

[9] A. Chaddad, C. Desrosiers, and M. Toews, "Phenotypic characterization of glioblastoma identified through shape descriptors," 2016, vol. 9785, p. 97852M–97852M–7.

[10] J. Lee et al., "Texture Feature Ratios from Relative CBV Maps of Perfusion MRI Are Associated with Patient Survival in Glioblastoma," *AJNR Am J Neuroradiol*, Oct. 2015.

[11] G. Castellano, L. Bonilha, L. M. Li, and F. Cendes, "Texture analysis of medical images," *Clinical Radiology*, vol. 59, no. 12, pp. 1061–1069, Dec. 2004.

[12] T. Upadhaya, Y. Morvan, E. Stindel, P. J. L. Reste, and M. Hatt, "Prognostic value of multimodal MRI tumor features in Glioblastoma multiforme using textural features analysis," in *2015 IEEE 12th International Symposium on Biomedical Imaging (ISBI)*, 2015, pp. 50–54.

[13] R. M. Haralick, K. Shanmugam, and I. Dinstein, "Textural Features for Image Classification," *IEEE Transactions on Systems, Man and Cybernetics*, vol. SMC-3, no. 6, pp. 610–621, Nov. 1973.

[14] V. Arvis, C. Debain, M. Berducot, and A. Benassi, "Generalization of the cooccurrence matrix for colour images: application to colour texture classification," *Image Analysis & Stereology*, vol. 23, no. 1, pp. 63–72, 2004.

[15] A. Chaddad and C. Tanougast, "Extracted magnetic resonance texture features discriminate between phenotypes and are associated with overall survival in glioblastoma multiforme patients," *Med Biol Eng Comput*, pp. 1–12, Mar. 2016.

[16] M. Vallières, C. R. Freeman, S. R. Skamene, and I. El Naqa, "A radiomics model from joint FDG-PET and MRI texture features for the prediction of lung metastases in soft-tissue sarcomas of the extremities," *Phys Med Biol*, vol. 60, no. 14, pp. 5471–5496, Jul. 2015.

[17] W. M. Wells, P. Viola, H. Atsumi, S. Nakajima, and R. Kikinis, "Multi-modal volume registration by maximization of mutual information," *Med Image Anal*, vol. 1, no. 1, pp. 35–51, Mar. 1996.

[18] Y. Liu, X. Xu, L. Yin, X. Zhang, L. Li, and H. Lu, "Relationship between Glioblastoma Heterogeneity and Survival Time: An MR Imaging Texture Analysis," *American Journal of Neuroradiology*, vol. 38, no. 9, pp. 1695–1701, Sep. 2017.

[19] D. Yang, G. Rao, J. Martinez, A. Veeraraghavan, and A. Rao, "Evaluation of tumor-derived MRI-texture features for discrimination of molecular subtypes and prediction of 12-month survival status in glioblastoma," *Medical Physics*, vol. 42, no. 11, pp. 6725–6735, Nov. 2015.

[20] F. W. Prior et al., "TCIA: An information resource to enable open science," *Conf Proc IEEE Eng Med Biol Soc*, vol. 2013, pp. 1282–1285, 2013.

[21] "3D Slicer." [Online]. Available: <http://www.slicer.org/>. [Accessed: 20-Oct-2014].

[22] R. M. Haralick, "Statistical and structural approaches to texture," *Proceedings of the IEEE*, vol. 67, no. 5, pp. 786–804, 1979.

[23] J. H. Zar, "Significance Testing of the Spearman Rank Correlation Coefficient," *Journal of the American Statistical Association*, vol. 67, no. 339, pp. 578–580, 1972.

[24] D. G. Kleinbaum and M. Klein, "Kaplan-Meier Survival Curves and the Log-Rank Test," in *Survival Analysis*, Springer New York, 2012, pp. 55–96.

[25] K. J. Archer and R. V. Kimes, "Empirical characterization of random forest variable importance measures," *Computational Statistics & Data Analysis*, vol. 52, no. 4, pp. 2249–2260, Jan. 2008.

[26] M. G. McNamara, S. Sahebjam, and W. P. Mason, "Emerging biomarkers in glioblastoma," *Cancers*, vol. 5, no. 3, pp. 1103–1119, 2013.

- [27] R. G. W. Verhaak *et al.*, "Integrated Genomic Analysis Identifies Clinically Relevant Subtypes of Glioblastoma Characterized by Abnormalities in PDGFRA, IDH1, EGFR, and NF1," *Cancer Cell*, vol. 17, no. 1, pp. 98–110, Jan. 2010.
- [28] H. Ohgaki *et al.*, "Genetic Pathways to Glioblastoma: A Population-Based Study," *Cancer Res*, vol. 64, no. 19, pp. 6892–6899, Oct. 2004.
- [29] H. S. Phillips *et al.*, "Molecular subclasses of high-grade glioma predict prognosis, delineate a pattern of disease progression, and resemble stages in neurogenesis," *Cancer Cell*, vol. 9, no. 3, pp. 157–173, Mar. 2006.
- [30] D. A. Gutman *et al.*, "Somatic mutations associated with MRI-derived volumetric features in glioblastoma," *Neuroradiology*, vol. 57, no. 12, pp. 1227–1237, Dec. 2015.
- [31] S. Holm, "A simple sequentially rejective multiple test procedure," *Scandinavian journal of statistics*, pp. 65–70, 1979.
- [32] Y. Nieto, F. Nawaz, R. B. Jones, E. J. Shpall, and S. Nawaz, "Prognostic significance of overexpression and phosphorylation of epidermal growth factor receptor (EGFR) and the presence of truncated EGFRvIII in locoregionally advanced breast cancer," *J. Clin. Oncol.*, vol. 25, no. 28, pp. 4405–4413, Oct. 2007.
- [33] K. D. Aldape *et al.*, "Immunohistochemical detection of EGFRvIII in high malignancy grade astrocytomas and evaluation of prognostic significance," *J. Neuropathol. Exp. Neurol.*, vol. 63, no. 7, pp. 700–707, Jul. 2004.
- [34] C. A. Del Vecchio *et al.*, "EGFRvIII gene rearrangement is an early event in glioblastoma tumorigenesis and expression defines a hierarchy modulated by epigenetic mechanisms," *Oncogene*, vol. 32, no. 21, pp. 2670–2681, May 2013.
- [35] P. Lambin *et al.*, "Radiomics: extracting more information from medical images using advanced feature analysis," *Eur. J. Cancer*, vol. 48, no. 4, pp. 441–446, Mar. 2012.
- [36] G. Lee, H. Y. Lee, E. S. Ko, and W. K. Jeong, "Radiomics and imaging genomics in precision medicine, Radiomics and imaging genomics in precision medicine," *Precision and Future Medicine, Precision and Future Medicine*, vol. 1, no. 1, pp. 10–31, Mar. 2017.
- [37] S. M. S. Reza, A. Islam, and K. M. Kiftekha@odu.edu, "Texture Estimation for Abnormal Tissue Segmentation in Brain MRI," in *The Fractal Geometry of the Brain*, A. D. Ieva, Ed. Springer New York, 2016, pp. 333–349.
- [38] F. Davnall *et al.*, "Assessment of tumor heterogeneity: an emerging imaging tool for clinical practice?," *Insights Imaging*, vol. 3, no. 6, pp. 573–589, Dec. 2012.
- [39] A. Kassner and R. E. Thornhill, "Texture analysis: a review of neurologic MR imaging applications," *AJNR Am J Neuroradiol*, vol. 31, no. 5, pp. 809–816, May 2010.
- [40] M. S. de Oliveira *et al.*, "MR imaging texture analysis of the corpus callosum and thalamus in amnesic mild cognitive impairment and mild Alzheimer disease," *AJNR Am J Neuroradiol*, vol. 32, no. 1, pp. 60–66, Jan. 2011.
- [41] P. Kickingereder *et al.*, "Radiomic Profiling of Glioblastoma: Identifying an Imaging Predictor of Patient Survival with Improved Performance over Established Clinical and Radiologic Risk Models," *Radiology*, vol. 280, no. 3, pp. 880–889, Jun. 2016.
- [42] P. Prasanna, J. Patel, S. Partovi, A. Madabhushi, and P. Tiwari, "Radiomic features from the peritumoral brain parenchyma on treatment-naïve multi-parametric MR imaging predict long versus short-term survival in glioblastoma multiforme: Preliminary findings," *Eur Radiol*, Oct. 2016.
- [43] M. Zhou, B. Chaudhury, L. O. Hall, D. B. Goldgof, R. J. Gillies, and R. A. Gatenby, "Identifying spatial imaging biomarkers of glioblastoma multiforme for survival group prediction," *J Magn Reson Imaging*, Sep. 2016.
- [44] M. Ingrisich *et al.*, "Radiomic Analysis Reveals Prognostic Information in T1-Weighted Baseline Magnetic Resonance Imaging in Patients With Glioblastoma," *Invest Radiol*, vol. 52, no. 6, pp. 360–366, Jun. 2017.
- [45] M. Inconorato *et al.*, "Radiogenomic Analysis of Oncological Data: A Technical Survey," *Int J Mol Sci*, vol. 18, no. 4, Apr. 2017.
- [46] Y. Cui, S. Ren, K. K. Tha, J. Wu, H. Shirato, and R. Li, "Volume of high-risk intratumoral subregions at multi-parametric MR imaging predicts overall survival and complements molecular analysis of glioblastoma," *Eur Radiol*, Feb. 2017.
- [47] M.-M. Inda, R. Bonavia, and J. Seoane, "Glioblastoma Multiforme: A Look Inside Its Heterogeneous Nature," *Cancers (Basel)*, vol. 6, no. 1, pp. 226–239, Jan. 2014.
- [48] C. C. Jaffe, "Imaging and genomics: is there a synergy?," *Radiology*, vol. 264, no. 2, pp. 329–331, Aug. 2012.
- [49] M. Diehn *et al.*, "Identification of noninvasive imaging surrogates for brain tumor gene-expression modules," *PNAS*, vol. 105, no. 13, pp. 5213–5218, Jan. 2008.
- [50] E. Sala *et al.*, "Unravelling tumour heterogeneity using next-generation imaging: radiomics, radiogenomics, and habitat imaging," *Clin Radiol*, vol. 72, no. 1, pp. 3–10, Jan. 2017.
- [51] H. Itakura *et al.*, "Magnetic resonance image features identify glioblastoma phenotypic subtypes with distinct molecular pathway activities," *Sci Transl Med*, vol. 7, no. 303, p. 303ra138, Sep. 2015.
- [52] L. S. Hu *et al.*, "Radiogenomics to characterize regional genetic heterogeneity in glioblastoma," *Neuro-oncology*, vol. 19, no. 1, pp. 128–137, Jan. 2017.
- [53] J. Lee *et al.*, "Texture Feature Ratios from Relative CBV Maps of Perfusion MRI Are Associated with Patient Survival in Glioblastoma," *AJNR Am J Neuroradiol*, vol. 37, no. 1, pp. 37–43, Jan. 2016.
- [54] P. Prasanna, J. Patel, S. Partovi, A. Madabhushi, and P. Tiwari, "Radiomic features from the peritumoral brain parenchyma on treatment-naïve multi-parametric MR imaging predict long versus short-term survival in glioblastoma multiforme: Preliminary findings," *Eur Radiol*, vol. 27, no. 10, pp. 4188–4197, Oct. 2017.
- [55] C.-X. Wu, G.-S. Lin, Z.-X. Lin, J.-D. Zhang, S.-Y. Liu, and C.-F. Zhou, "Peritumoral edema shown by MRI predicts poor clinical outcome in glioblastoma," *World J Surg Oncol*, vol. 13, Mar. 2015.
- [56] A. Chaddad, C. Desrosiers, L. Hassan, and C. Tanougast, "A quantitative study of shape descriptors from glioblastoma multiforme phenotypes for predicting survival outcome," *BJR*, vol. 89, no. 1068, p. 20160575, Oct. 2016.
- [57] S. Liu *et al.*, "Relationship between necrotic patterns in glioblastoma and patient survival: fractal dimension and lacunarity analyses using magnetic resonance imaging," *Sci Rep*, vol. 7, Aug. 2017.
- [58] D. A.-S. Michel Lacroix, "A multivariate analysis of 416 patients with glioblastoma multiforme: prognosis, extent of resection, and survival," *Journal of neurosurgery*, vol. 95, no. 2, pp. 190–8, 2001.
- [59] R. Jain *et al.*, "Outcome Prediction in Patients with Glioblastoma by Using Imaging, Clinical, and Genomic Biomarkers: Focus on the Nonenhancing Component of the Tumor," *Radiology*, vol. 272, no. 2, pp. 484–493, Aug. 2014.
- [60] M. Park *et al.*, "Elderly patients with newly diagnosed glioblastoma: can preoperative imaging descriptors improve the predictive power of a survival model?," *J Neurooncol*, vol. 134, no. 2, pp. 423–431, Sep. 2017.

Appendix 1

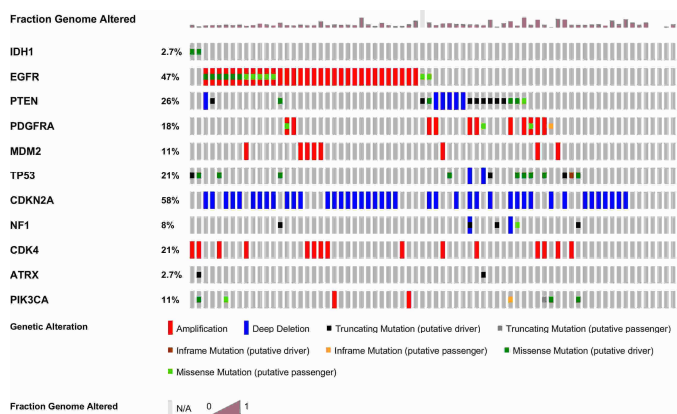


Fig. 1 S. Genomic landscape of the cohort of 73 patients used in this study. Copy number alteration and mutational changes for a range of the most commonly mutated genes in GBM are shown.

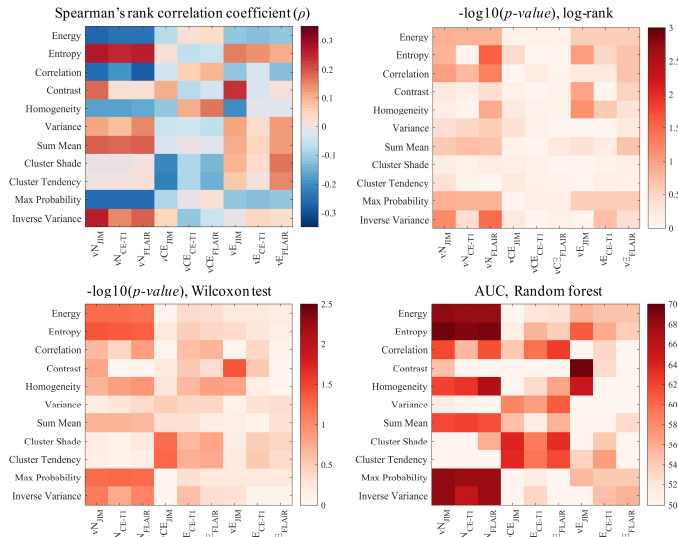


Fig. 4 S1. Analysis of texture features derived from uncensored GBM patients (n=63). See Fig. 4 for a detailed description.

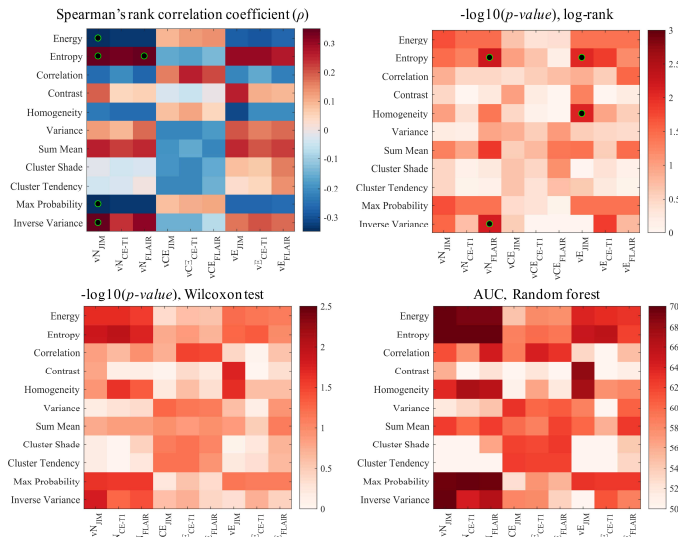


Fig. 4 S2. Analysis of texture features derived from GBM patients that received radiation treatment (n=61). See Fig. 4 for a detailed description.

Table IV.S

SUMMARY OF KAPLAN-MEIER ANALYSIS FOR SIGNIFICANT FEATURES (I.E., CORRECTED $P < 0.05$) DERIVED FROM NECROSIS AND EDEMA REGIONS FOR GBM PATIENTS THAT RECEIVED RADIATION TREATMENT (N=61).

GBM region	Features / JIMs	Cut-off	MS (days)	
			Feature > Cut-off	Feature < Cut-off
Necrosis	Entropy/FLAIR	0.34	451.5	333
	Inverse-variance/FLAIR	0.03	451.5	333
Edema	Entropy/JIM	0.276	530	330.5
	Homogeneity/JIM	0.934	288	530

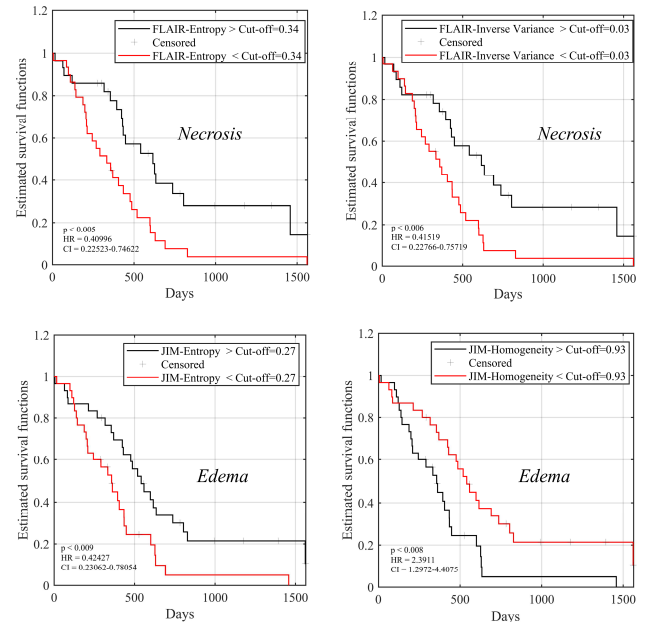


Fig. 6 S1. Kaplan-Meier curves comparing the survival rate of GBM patients that received radiation treatment (n=61), partitioned into two groups using cut-off (median) of the significant features. Features derived from necrosis (Top) and edema (Bottom) regions as depicted in Figure 4 S2 (Top Right).

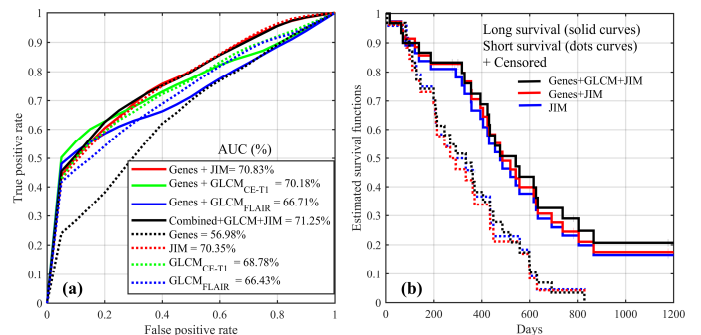


Fig. 5 S2. Survival analysis for GBM patients that received radiation treatment (n=61). (a) Mean ROC curves obtained by the RF model for discriminating between short and long survival time patients (using the median survival time as threshold). Results are reported for various imaging features and combinations of genomic, JIM and GLCM features. (b) Kaplan-Meier curves comparing the survival rate of patient groups predicted by the random forest classifier using different feature combinations as input.

TABLE V. S1

SUMMARY OF KAPLAN-MEIER ANALYSIS FOR PREDICTED PATIENTS (GBM PATIENTS THAT RECEIVED RADIATION TREATMENT (N=61)) GROUPS (I.E., SHORT VS. LONG SURVIVAL OUTCOME). THE MEDIAN SURVIVAL (MS) TIME, HAZARD RATIO (HR), 95% CONFIDENCE INTERVAL (CI) AND LOG-RANK P-VALUE ARE REPORTED.

Features	MS (days)		HR	CI	p
	short	long			
Genes + JIM	279.5	476	2.71	1.4-5.0	0.003
Genes + GLCM-CE-T1	357	441	1.58	0.89-2.8	0.150
Genes + GLCM-FLAIR	362	427	1.54	0.88-2.6	0.161
Genes + GLCM + JIM	333	465.5	2.58	1.4-4.6	0.002
Genes	357	432	1.73	0.9-3.2	0.131
JIM	300.5	455	2.35	1.2-4.3	0.011
GLCM-CE-T1	366	424	1.15	0.67-1.9	0.718
GLCM-FLAIR	358	432	1.63	0.91-2.8	0.128

TABLE V. S2
SUMMARY OF KAPLAN-MEIER ANALYSIS FOR PREDICTED PATIENTS (N=73)
GROUPS (I.E., SHORT VS. LONG SURVIVAL OUTCOME) USING LOOCV

<i>Features</i>	<i>MS (days)</i>		<i>HR</i>	<i>CI</i>	<i>p</i>
	short	long			
Genes + JIM	268	444.5	1.93	1.1-3.1	0.01
Genes + GLCM-CE-T1	333	409.0	1.14	0.7-1.8	0.68
Genes + GLCM-FLAIR	358	375.5	1.45	0.8-2.3	0.16
Genes + GLCM + JIM	268	465.5	2.86	1.6-5.0	0.0004
Genes	358	374.5	1.23	0.7-1.9	0.47
JIM	322	429.0	1.88	1.1-3.1	0.02
GLCM-CE-T1	328	427.0	1.42	0.87-2.3	0.19
GLCM-FLAIR	330.5	424.0	1.42	0.87-2.3	0.19